A&A, 687, A134 (2024)
https://doi.org/10.1051/0004-6361/202450281

Astronomy & Astrophysics

Radar observation of the new λ-Sculptorid meteor shower

D. Janches[1], J. S. Bruzzone[2,3], E. C. M. Dawkins[1,4], R. Weryk[5], J. D. Carrillo Sanchez[1,4], A. Egal[5,6,7], G. Stober[8], J. L. Hormaechea[9], D. Vida[5], and C. Brunini[10]

[1] Space Weather Laboratory, NASA Goddard Space Flight Center, Greenbelt MD USA
e-mail: diego.janches@nasa.gov
[2] Facultad de Ciencias, Universidad de la Republica, Montevideo, Uruguay
[3] Centro Universitario Regional del Este, Universidad de la Republica, ruta nacional 9 y ruta 15, Rocha 27000, Uruguay
[4] Department of Physics, Catholic University of America, DC, USA
[5] Department of Physics and Astronomy, The University of Western Ontario, London, Ontario, Canada
[6] Planetarium de Montreal, Montreal, Quebec, Canada
[7] IMCCE, Observatoire de Paris, Paris, France
[8] University Bern, Institute of Applied Physics, Microwave Physics, Bern, Switzerland
[9] Estacion Astronomica Rio Grande, Rio Grande, Tierra del Fuego, Argentina
[10] Investigador independiente, Buenos Aires, Argentina

Received 8 April 2024 / Accepted 21 May 2024

ABSTRACT

Context. 46P/Wirtanen is a near-Earth comet (NEC) and several previous modeling works had predicted it would produce a meteor shower for the first time on December 12, 2023.

Aims. We report the most comprehensive meteor radar observations of the λ-Sculptorid meteor shower produced by comet 46P/Wirtanen. These measurements are critical to constrain the mass distribution of the particles released by the comet as radars generally detect the smaller particle population of the shower.

Methods. We utilized observations with the Southern Argentina Agile Meteor Radar-Orbital System (SAAMER-OS) ideally located in the southern hemisphere to detect this shower. Since the shower was predicted to produce very slow meteors, we used the same methodology applied for the Arid meteor shower.

Results. As predicted, the shower peak was observed by SAAMER-OS on December 12, 2023 ($\lambda_0 = 259.73°$) at 0900 UTC, with a Zenithal Hourly Rate (ZHR) peak value of ~2.5 m h^{-1}. Most of the activity of the shower was observed during 2 h between 0730–0930 UTC. The observed mean radiant of the shower in Sun-centered ecliptic coordinates is located at $\lambda - \lambda_0 = 88.9°$ and $\beta = -36.6°$. Our results suggest that the particles detected by SAAMER-OS are in general larger than those for which thermal equilibrium can be assumed (>3 mg) in agreement with the conclusions of previous reports using video observations.

Key words. meteorites, meteors, meteoroids – zodiacal dust – comets: individual: λ-Sulptorid

1. Introduction

Comet 46P/Wirtanen, a Jupiter family comet (JFC) discovered in January 1948 by C. Wirtanen at Lick Observatory, experienced close encounters with the giant planet in 1972 and 1984. In 2018, the comet's orbit was within 0.077 au from Earth, during which it was characterized as a hyper-active comet (Moulane et al. 2023). Given its orbit proximity to that of Earth, this comet can potentially be the parent of a meteor shower (Ye & Jenniskens 2022). In fact, Maslov & Muzyko (2017) reported a search of possible showers from the modeling of the associated meteoroid stream but no observations were reported to confirm such predictions. Farnham et al. (2019) reported the detection of a faint optical trail observed by the Transiting Exoplanet Survey Satellite (TESS), despite the fact that previous observations of the dust trail with the InfraRed Astronomy Satellite (IRAS) and Spitzer yielded null results.

Vaubaillon et al. (2023) revisited the potential meteor shower parenthood of 46P and found several past encounters between Earth and the potential stream produced by the comet, predicting the birth of the λ-Sculptorid meteor shower (since the predicted location of the radiant is close to the λ-Sculptoris star). According to that work, the shower would occur on December 12, 2023, between 08:00 and 12:30 UT, with the maxima time depending on the size-frequency distribution of the ejected particles. Furthermore, the authors point out that both the lack of observations of a shower related to 46P is probably due to the unusual ejection velocity needed to bring large particles to the Earth, and the observation of such a shower may be difficult due to the low entry velocity (i.e. just under the escape velocity) and the relatively small sizes of the meteoroids, which makes these meteors hard to observe due to the rapidly decreasing luminous and ionization efficiencies at such low speeds.

A similar challenge occurred with the Arid meteor shower produced by comet 15P/Finlay, which was predicted to occur on September 29 2021, and a second more dominant peak on October 7 2021. According to modeling results, these peaks were derived from two major outbursts of activity during the comet's perihelion passage between December 2014 and January 2015 (Vaubaillon et al. 2020; Ye et al. 2021). The shower was successfully observed by the Southern Argentina Agile Meteor Radar-Orbital System (SAAMER-OS), reported by Janches et al. (2023). In that case, the time of occurrence of the two detected peaks was in good agreement with the predictions for this shower, confirming the validity of the model used for the calculations.

As pointed out by Vaubaillon et al. (2023), reporting the observation of this new shower is of critical importance since it constrains dynamical models as well as the size-frequency distribution of large particles for parent bodies. In fact, Vida et al. (2024) recently reported the observation of the λ-Sculptorid shower using video observations in Australia, New Zealand, and the rest of Oceania with the Global Meteor Network video cameras. The authors reported a total of 23 λ-Sculptorid orbits, peaking at a zenithal hourly rate (ZHR) of $0.65^{+0.24}_{-0.20}$ meteors per hour at $\lambda_0 = 259.988 \pm 0.042°$. The estimated low in-atmosphere speed of 15 $\mathrm{km\,s^{-1}}$ resulted in an estimated mean mass of observed meteoroids of 0.5 g (∼10 mm diameter), an order of magnitude higher than predicted. The authors used dynamical simulations of the meteoroid stream and concluded that these particles must have a very low bulk density of ∼100 $\mathrm{kg\,m^{-3}}$ for such large meteoroids to encounter Earth in 2023 with the predicted radiant. However, this assumption of a low bulk density cannot explain completely the measured activity profiles. In addition, as shown in Vondrak et al. (2008) (see their Fig. 15), even though particles with comparatively low density start releasing their metal constituents several km higher than those particles with a more compact nature, the ablated fraction of metals decrease significantly in the case of bodies with a porous structure, leading consequently to lower ionization profiles in the upper atmosphere.

Similar to the Arid meteor shower, SAAMER-OS successfully observed the λ-Sculptorid meteor shower, and the results are reported here. Radar observations generally observe smaller particles than those observed by optical video networks and thus, these results complement very well with the observations reported by Vida et al. (2024). However, unlike the case of the Arids which resulted in sufficient statistics in order to estimate mean orbits, fluxes, and mass indices, for the case of the λ-Sculptorid, only up to 25 meteors were observed, depending on how far from the predicted radiant center is considered, which limits the comparisons that can be made with the modeled results. As is subsequently discussed in this paper, fewer detections may be an indication that this shower is composed of larger particles than those forming the Arid meteor shower, which is in agreement with the conclusions reported by Vida et al. (2024).

2. Instrumentation and data analysis

SAAMER-OS characteristics have been described by many previous works (Janches et al. 2015, 2020, 2023; Bruzzone et al. 2020, 2021). In most of the cases, each report described newer upgrades performed to this ever-evolving system. Specific to this report, SAAMER-OS is a six-station Very High Frequency (VHF) meteor pulse radar located in Rio Grande, Tierra del Fuego, Argentina. The central station (SAAMER-C; 53.786° S, 67.751° W) hosts the single crossed-element transmitting antenna and five crossed-element antenna interferometric receiving array. The central station also hosts two additional single-element antennas, which make perpendicular measurements of the polarization of each returned echo. This was added to the system to better constrain mass determinations for each single detection (Stober et al. 2023; Dawkins et al. 2023). In addition, to define the Orbital System, SAAMER has five additional receiving stations which are each composed of single crossed-element antennas for time-of-flight velocity determinations from near-backscattering: SAAMER-N (53.682° S, 67.871° W, ∼13 km northwest); SAAMER-W (53.828° S, 67.842° W, ∼7 km southwest); SAAMER-S (53.852° S, 67.76° W, ∼7 km south); SAAMER-E (53.772° S, 67.727° W, ∼4 km northeast); and SAAMER-SE (53.804° S, 67.676° W, ∼5 km southeast). The radar transmits with a peak power of 64 kW at 32.55 MHz using a pulse repetition frequency of 625 Hz.

Because of the characteristically low speed of the potential λ-Sculptorid meteor shower, we performed a similar analysis to that used for the Arid shower (Janches et al. 2023). In that work, it was found that deceleration and measurement uncertainty can cause the apparent in-atmosphere speed to be too low such that the computed geocentric speed is undefined. This prevents the determination of a heliocentric orbit. Additional detection difficulties of a slow shower are caused by the fact that the ionization efficiency is heavily dependent on the meteoroid velocity (Weryk & Brown 2013), since radars detect the ionization left behind by a meteoroid's ablation (i.e. meteor), and thus trails may not be dense enough to be detected.

Similarly to our previous reported searches, we employ a 3-D wavelet transform algorithm to precisely determine the radiant of the events for which defined geocentric speeds were obtained. The 3-D wavelet transform in $(\lambda - \lambda_0, \beta, v_g)$ is a well-proven technique to associate radar meteors to meteor showers (Baggaley et al. 1994; Brown et al. 2008, 2010; Bruzzone et al. 2015, 2020; Pokorný et al. 2017; Schult et al. 2018), where λ and β are the ecliptic longitude and latitude, λ_0 is the solar longitude and v_g is the geocentric speed. When this technique is applied to a given meteor distribution, a wavelet coefficient w_c is obtained which increases with the clustering of meteors in Sun-centered ecliptic coordinated $(\lambda - \lambda_0, \beta, v_g)$ as showers display characteristic scales in time domain and radiant space. The wavelet kernel is chosen to enhance scales in phase space typical of showers, and is therefore not sensitive to the more diffuse meteor sporadic background (Bruzzone et al. 2015). We thus conduct the search for the w_c local maximum on December 12th, 2023 ($\lambda_0 = 259.9°$ at 12 UTC). The wavelet transform is evaluated at 0.1° steps in $\lambda - \lambda_0$ and β, and at 1% steps in geocentric speed. These events with a defined geocentric speed allow us to determine heliocentric Keplerian orbits which we then combine into an average stream orbit.

3. Results

Unlike the case of the Arid meteor shower (Janches et al. 2023), SAAMER-OS did not detect an outburst of activity. Furthermore, the radar did not observe a clear detection as only a few meteors (∼25) were found within the expected radiant (Fig. 1). The left panel of Fig. 2 shows that the events were detected around the predicted shower radiant mostly spread over a period of 14 h. However the peak activity of the shower occurs at 0900 UTC of December 12th, 2023 ($\lambda_0 = 259.73°$) and most of the activity is recorded during a 2 h period at 0800 and 0900 UTC (SAAMER-OS results have a resolution of 1 h). Although this appears to be in general good agreement with the activity period reported by Vida et al. (2024) there is a marked difference between the time of the peak activity between the radar observations and those recorded by video techniques ($\lambda_0 = 259.98°$, 1505 UTC 2023 December 12). However, even though the collected statistics are not optimal for a definite result, this peak time is within the predicted range by Vaubaillon et al. (2023). When looking at the data in detail, we found that out of the 25 events several had larger velocities than expected, or some seem to have been detected at too low height (∼40 km), and thus we applied an additional filter and consider only those events with measured speeds between 8 and 13 $\mathrm{km\,s^{-1}}$. Note that there

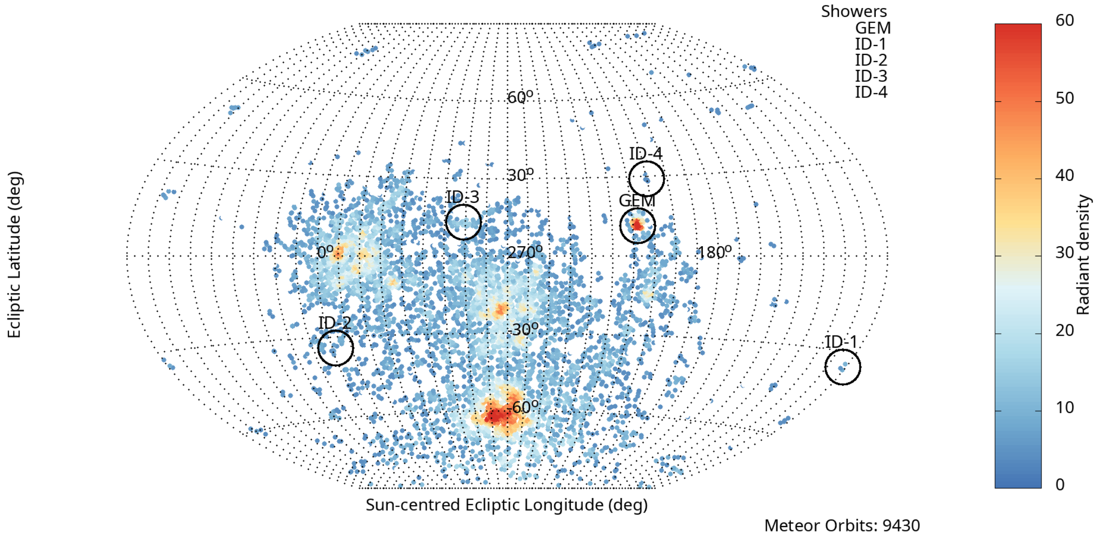

Fig. 1. Sun-centered meteoroid radiants detected by SAAMER-OS on December 12th (λ_0 = 259.9°), 2023, color coded by radiant density. The black circles labeled ID 1–4 are locations where the wavelet code detects potential presence of an enhancement of non-identified meteor showers. Specifically, ID-1 is the location where the λ-Sculptorid shower was predicted to occur. The center of the enhancement is located at $\lambda - \lambda_0 = 91.5°$ and $\beta = -35.0°$.

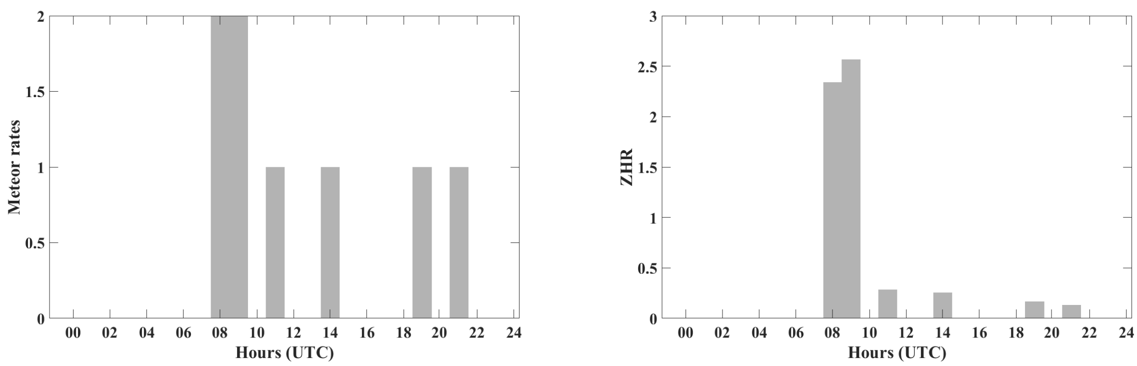

Fig. 2. SAAMER-OS Detected Statistics. Left: Number of detected meteors as a function of time within the 10° of the λ-Sculptorid radiant during the time of the predicted outbursts. Right: Estimated ZHR.

are two ways SAAMER-OS calculates the altitude. The traditional one solely based on detected range and interferometry angle (Fritts et al. 2010). The other one based on the trajectory calculation and if the velocity solution is incorrect because of the time pick of the t_0 point is wrong, it will corrupt the altitude estimate (Janches et al. 2023). Overall, there are very few meteors with this issue (1 or 2 a day when selecting specific shower radiants). In addition, we analyzed the data considering the events that were detected within 10, 15, and 20° of the reported radiant.

In order to investigate the potential contamination of sporadics we extract meteors at 10 and 20 degrees in the sky from the position of the shower radiant five degrees of solar longitude before and after from the recorded peak. Table 1 shows the number of meteors with v_g between 8 and 13 km s^{-1} (n) and the amount of total meteors present (N, i.e. without filtering in speed). For example, during the peak ($\Delta\lambda_0 = 0$) there are 8 meteors identified as members of the shower from a total of 10 at a selection radius of 10° and 12 out of a total of 22 for a selection radius equal to 20°. The small contamination of sporadics can also be seen in Fig. 3 where we show the radiant of the meteors for selection radii of 10° (top panel) and 20° (bottom panel). The meteors identified as members of the shower are colored blue and it is clear that they are the majority of the detected events.

The results of the estimated peak ZHR, for the case of the most restricted selection (10° aperture), are shown in Fig. 2 (right panel) with a mass index of 2.2 as in Vida et al. (2024). Figure 2 presents histograms of meteor detected rates (left panel) and estimated ZHR (right panel) for those meteors within 10° of the RA = 7.3° and δ = −38.5°. In order to estimate the ZHR we first determine the flux at the detection limiting magnitude of 9 which results in 0.0378 km^{-2} h^{-1}. We then convert this flux to a standard limiting magnitude of 6.5 which results in 0.00239 km^{-2} h^{-1} and use this value to estimate the peak ZHR = ~2.56 meteors per hour. It is important to note that the fluxes are corrected by the Radar Response Function (RRF) as described in Janches et al. (2015) and Bruzzone et al. (2021). The value is almost four times higher than the peak ZHR of 0.65 reported by Vida et al. (2024) with the same mass index value (s = 2.25). The only way to reconcile both sets of observations is by allowing a steeper mass index (e.g., 2.45–2.5). In that case, SAAMER-OS' resulting peak ZHR decreases to ~0.5 if s = 2.5, which is well within the wide 95% confidence interval of [1.73, 3.75] found by Vida et al. (2024). As the ionization efficiency rapidly changes at these low speeds, scaling the flux to a single reference mass is very sensitive to even the smallest errors in the speed measurements, which

Table 1. Sporadic contamination results.

$\Delta\lambda_0$ (°)	10°		20°	
	n	N	n	N
–5	1	5	4	12
–4	0	2	5	13
–3	1	1	3	12
–2	2	4	12	23
–1	0	6	4	18
0	8	10	12	22
+1	2	10	6	24
+2	2	8	11	24
+3	1	2	1	2
+4	3	6	9	28
+5	1	2	5	14

Notes. Number of meteors with v_g between 8 and 13 km s^{-1} (n) and the amount of total meteors present (N) for two selection radii.

may explain the difference in the flux. Alternatively, it is possible due to the significantly different observed period (the radar peak was observed ~6 h before the video peak) that two distinct populations were observed with different mass distribution indices. Unfortunately, the small number statistics prevents us from independently measuring a meaningful value of the mass index.

Unfortunately, at this stage, the ZHR values derived using SAAMER-OS observations do not have errors since we have yet to develop a methodology to estimate errors on several products of the radar. Bruzzone et al. (2020) indicated that the average uncertainty of the radiant is lower than a degree. This was performed for several showers observed using SAAMER-OS and Cameras for Allsky Meteor Surveillance (CAMS, Jenniskens et al. 2011). Specifically, the average radiant position uncertainty is 0.60° and 0.63° with average speed uncertainties of 0.24 km s^{-1} and 0.03 km s^{-1} for SAAMER-OS and CAMS observations respectively.

Table 2 lists the orbital parameters determined from SAAMER-OS observations for samples obtained within 10, 15, and 20° from the center of the predicted radiant and are compared to the results obtained by Vida et al. (2024). Although overall, our orbital results seem to agree very well with those estimated by Vida et al. (2024) there is a significant shift in the peak time, probably due to the mass sorting in the orbit. We note again that Vida et al. (2024) results in principle, represent particles significantly larger than those detected by SAAMER-OS.

Although mass determination for meteor observations is critical in general, it is even more important for the case of this shower since both the earlier predictions by Vaubaillon et al. (2023) and the observations reported by Vida et al. (2024) show a conflicting combination of slow ejection velocities, large masses and reported and predicted activity profiles. For this task, we used the methodology recently developed at SAAMER-OS and reported by Stober et al. (2023) and Dawkins et al. (2023). Through this new method, we utilized the new polarization measurements at SAAMER-OS to determine the electron line density of each detected meteor with the help of a Full Wave Scattering model (Stober et al. 2023). We then used that quantity, together with the measured meteor velocity, altitude, and entry angle to determine the initial mass and velocity of the particle. For this second step, we produce a 3-D interpolation of a subset

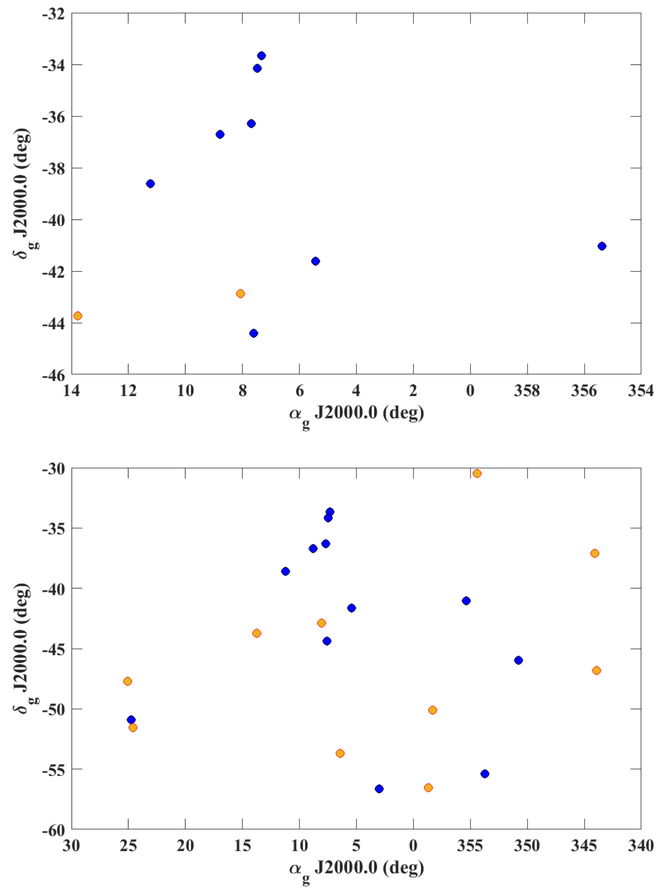

Fig. 3. Detected radiants for meteors within 10° (top) and 20° (bottom) from the shower radiant. Blue circles are those events identified as members of the shower.

of simulated electron density profiles, derived by the Chemical Ablation model (CABMOD; Vondrak et al. 2008) combined with a model that predicts the primary ionization profiles of ablated meteoric metals produced by hyperthermal collisions with air molecules. For this purpose, we select the profile that best matches the particle's detected velocity (v_s), and electron line density (q_s) at the altitude of detection (z_s) within certain threshold criteria, for a given entry angle. It is important to note that at this stage CABMOD does not include a treatment of fragmentation which could eventually affect some of these results.

For the case of the λ-Sculptorid events, we can successfully apply this methodology for 2 out of the 21 detected particles (for this portion of the study we are also using particles with atmospheric initial velocities greater than 13 km s^{-1}). These two cases are listed in Table 3. The subscript "s" indicates the variables at the time and altitude of detection by SAAMER-OS, while the subscript "i" indicates the estimated values at the top of the atmosphere. The standard error is presented where applicable; this was computed using a 1000-sample Monte Carlo simulation which perturbed the detected v_s by ±0.5 km s^{-1}, z_s by ±0.5 km, and q_s by ±15%.

For the rest of the events, there is no overlap between CABMOD and the detected particles and, consequently, neither 3-D interpolation nor the estimate of the initial mass and velocity of the particle can be derived. Figure 4 shows two examples of this disagreement, in which the filled red square denotes the particle q_s and v_s at altitude z_s (i.e. the measured altitude and velocity

Table 2. Orbital elements determined with SAAMER-OS observations.

	10°	15°	20°	Vida et al.
v_g (km s^{-1})	9.805 ± 1.322	9.6167 ± 1.3597	9.7645 ± 1.4358	
a (au)	2.9761 ± 0.8517	2.8719 ± 0.85588	2.769 ± 0.824	2.891
e	0.6485 ± 0.0851	0.63411 ± 0.090581	0.620 ± 0.095	0.66
i (°)	8.8175 ± 1.481	8.6989 ± 1.4301	9.425 ± 2.285	9.20
q (au)	0.98413 ± 0.00064	0.98378 ± 0.0012019	0.983 ± 0.002	0.985
ω(°)	0.72 ± 2.7	359.71 ± 3.9	359.18 ± 4.88	359.92
Ω(°)	79.61 ± 0.22	79.5722 ± 0.23398	79.5636 ± 0.2111	79.93
# of orbits	8	9	11	21

Notes. The SAAMER-OS results are samples obtained within 10, 15, and 20° from the center of the predicted radiant. The SAAMER-OS Results are also compared to the results obtained by Vida et al. (2024).

Table 3. Results for the two particles for which the mass determination methodology could be implemented.

Variable	P1	P2
z_s (km)	90.12	90.35
θ(°)	31.30	20.20
v_s (km s^{-1})	17.24	17.32
v_i (km s^{-1})	17.50 ± 0.01	17.50 ± 0.01
% of decel.	1.49	1.03
m_s (µg)	603.40 ± 31.54	666.66 ± 33.09
m_i (µg)	691.27 ± 31.40	750.74 ± 33.19
% mass loss	12.71	11.20

and the estimated line density at the moment of detection following the treatment presented in Stober et al. 2023). Moreover, the black data points in Fig. 4 represent the q versus v values of all CABMOD profiles at z_s. Note that CABMOD assumes that particles with masses <2774 µg stay isothermal for temperatures up to 2000 K for a CI-chondritic composition (Dawkins et al. 2023) and, therefore, the present study is not extended to larger bodies. The CABMOD results shown in Fig. 4 infer that particles with the entry angle, v_s and q_s observed by SAAMER-OS should have ablated completely at the measured altitude z_s (i.e. not producing any ionization such that q=0 e$^-$/m). As a result, the majority of the Wirtanen particles detected by SAAMER-OS exceed the mass range assumed by the CABMOD model, with masses potentially greater than ∼0.3 g and in agreement with the findings of Vida et al. (2024).

4. Comparison with a dynamical model

Numerical simulations were conducted using the model developed by Egal et al. (2019). Approximately 1.36 million particles were ejected from comet 46P/Wirtanen during each apparition since 1830. To enhance the precision of the comet's trajectory since 1830 and mitigate uncertainties (cf. Vaubaillon et al. 2023), we integrated its motion using all orbital solutions provided by JPL between 1947 (SAO/1947) and 2018 (K243/4), building the ephemeris of each apparition of the comet from the closest available orbital solution.

Particles were released daily from the sunlit hemisphere of the nucleus for heliocentric distances below 3 AU, following the ejection velocity model of Crifo & Rodionov (1997). The simulated meteoroids were distributed equally across radius bins [10^{-4}, 10^{-3}] m, [10^{-3}, 10^{-2}] m, and [10^{-2}, 10^{-1}] m, assuming a density of 1000 kg m^{-3}. While optical observations yield lower density measurements of the shower, dynamical models of the stream indicate that the radiant and arrival times of the simulated particles remain unaffected by the density assumption (Vida et al. 2024).

After ejection, the simulated trails were integrated forward in time, and the characteristics of Earth-impacting particles were analyzed. In the model, only particles crossing the ecliptic plane within a distance ΔX and time ΔT from the Earth are retained as potential impactors. In order to compute realistic meteoroid flux, each particle is assigned a weight reflecting the number of meteoroids that would have been released by 46P under similar circumstances (Egal et al. 2020). The tunable parameters of this weighting scheme, such as the selection parameters (ΔX, ΔT) or the meteoroids size distribution index, are determined though calibration of the modelled activity profile against observations of the λ-Sculptorid.

In this work, we have tried to find a weighting scheme for the simulations (including the particles' size distribution and particle selection), that would explain both SAAMER-OS measurements and Global Meteor Network (GMN) observations presented by Vida et al. (2024). Unfortunately, a single solution for the shower that would explain both set of measurements was not found. However, this discrepancy might provide some insight about what happened for the λ-Sculptorid complex in 2023.

Vida et al. (2024) questioned the implication of the 1974 trail, which matched well the observed radiant location but failed in reproducing the peak time and activity profile reported by GMN. In contrast, the authors found that by slightly releasing the timing and distance selection of the particles, they were able to bring some mm-sized particles close to the Earth at the right time. But the observations did not really help discriminate between these two options.

Figure 5 compares the fluxes observed by SAAMER, GMN and those from the dynamical models. In both panels of the figure, we see that the maximum peak observed with the radar occurred a few hours earlier than what recorded with the optical cameras, providing additional constraints to the dynamical models of the λ-Sculptorid stream.

The left panel of Fig. 5 presents the activity computed from all the particles that approached the Earth within ΔX = 0.02 AU and ΔT = 20 days. Particles of a few millimeters in size ejected from the comet prior to 1900 are found to produce most of this modelled activity, with a negligible contribution from the 1974 trail. We find the solution to be in good agreement with the peak time, activity, and mean radiant location reported by the video cameras (cf. Figs. 5 and 6). However, the model does not

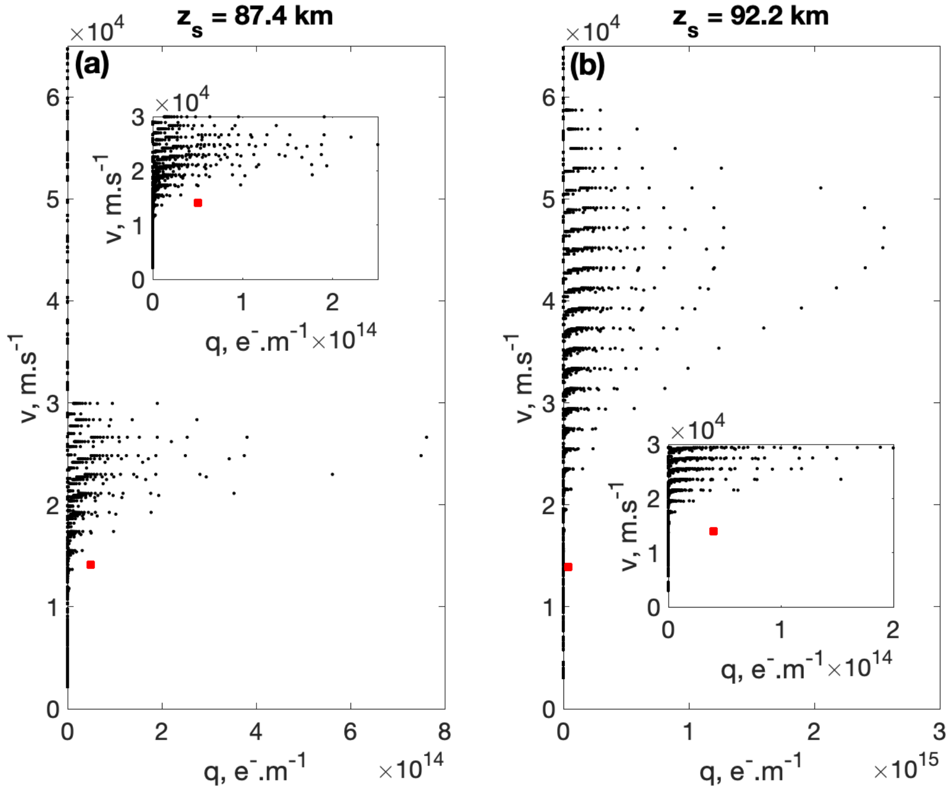

Fig. 4. Two detected example in which the mass determination methodology did not work. Left: the filled red square denotes the particle q_s and v_s at altitude z_s. The black data points represent the q versus v values of all CABMOD profiles at z_s. For the particle mass range that CABMOD uses (<2774 µg), CABMOD predicts that a particle with an entry angle, v_s and q_s matching the particle should have completely ablated at z_s (i.e. not producing any ionization such that q=0 e^- m^{-1}). The insert boxes are a zomm in of the portion of the figure around the red dots. The periodic pattern in the modeled results is due to the resolution in v, m and α of CABMOD.

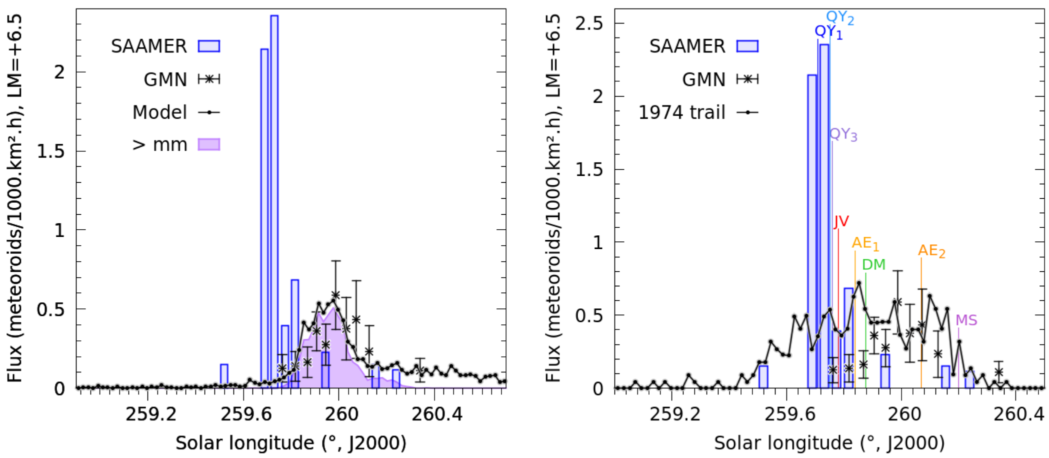

Fig. 5. Comparison of the λ-Sculptorid flux observed by SAAMER (blue boxes) and GMN (black symbols) in 2023. The meteoroid fluxes measurements provided in Vaubaillon et al. (2023); Vida et al. (2024) are compared with the modelled flux, when retaining particles that approached the Earth within ΔX = 0.02 AU (left panel) or ΔX = 0.005 AU (right panel). Coloured lines indicate the maximum activity time predicted by the different models of Vaubaillon et al. (2023), marked by the initials of the co-authors. While only small particles from the 1974 were retained in the second scenario, mm-sized particles ejected from the comet prior to 1900 were found to approach the Earth within 0.02 AU (pink area in the left panel). Both dynamical models suggest that if larger particles from older trails provide a good match with the activity reported by GMN, smaller particles from the 1974 trail are necessary to explain the first peak detected by SAAMER.

reproduce the timing and magnitude of the first peak observed by SAAMER-OS.

The right panel of Fig. 5 presents the flux obtained with a more restrictive distance selection criterion (ΔX = 0.005 AU). In this model, only small particles belonging to the 1974 trail were retained for the computation. While the modelled profile does not reproduce the magnitude of the first peak recorded by SAAMER-OS, the simulated profile allows explaining the shower timing, duration and average intensity. Our results thus suggest that most meteoroids detected by the radar were released by the 1974 trail, as predicted by Vaubaillon et al. (2023). The detection of the first activity peak around λ_0 = 259.73° reported by SAAMER, is in particular good agreement with the prediction of Ye et al. (2016).

The ecliptic radiants observed by SAAMER-OS are compared with GMN and the dynamical models in Fig. 6. Since both models result in very similar radiants structure, only one set of simulated positions obtained for the 1974 trail (filled circles) was included in the figure. We observe that the radiants measured by SAAMER are also very consistent with GMN and the observations from the Canadian Meteor Orbit Radar presented in Vida et al. (2024).

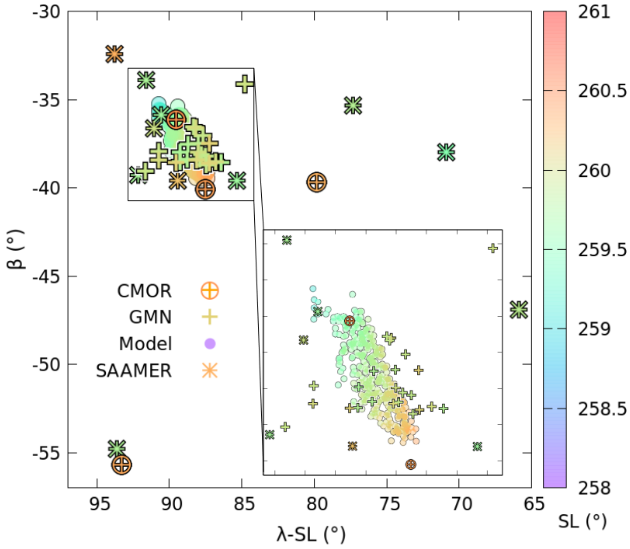

Fig. 6. Sun-centered ecliptic coordinates of the radiants measured by SAAMER, CMOR, GMN, and a dynamical model of the λ-Sculptorid stream. The radiant structure between 83° and 93° in longitude and –34° and –41° in latitude is zoomed in the bottom right of the plot.

While the contribution of older trails, modelled with larger (but still plausible) particles selection criteria are necessary to reproduce the GMN profile, our results indicate that a significant contribution from the 1974 trail is necessary to explain the radar observations.

5. Conclusions

We report the most comprehensive radar observation of the λ-Sculptorid meteor shower to date produced by comet 46P/Wirtanen, a near-Earth comet belonging to the JFC family. Vaubaillon et al. (2023) predicted the birth of the λ-Sculptorid meteor shower on December 12, 2023, between 8:00 and 12:30 UT, with the maxima time depending on the size-frequency distribution of the ejected particles. In this work, we utilized observations with SAAMER-OS which is ideally located in the southern hemisphere, where the shower was predicted to have the best observing chances given its southern ecliptic radiant. Since the shower is predicted to produce very slow meteors, we used the same methodology applied to the Arids meteor shower described in Janches et al. (2023). As predicted, the shower was observed by SAAMER-OS on December 12, 2023 (λ_0 = 259.73°) at 0900 UTC, with a ZHR peak value of ~2.5 meteors per hour. The measured mean radiant in Sun-centered ecliptic coordinates of the shower is located at $\lambda - \lambda_0$ = 88.9° and β = –36.6°. Results suggest that the particles detected by SAAMER-OS are in general larger than usually detected by radars which are those for which can be assumed that ablation occured under isothermal conditions (<3 mg). This result is in agreement with the conclusions reported by Vida et al. (2024) using video observations, with the marked difference that the radar peak was observed ~6 h prior to the video peak. In general, the orbital results are also in agreement with the video observations and modeled results (Vaubaillon et al. 2023), however, SAAMER-OS' estimated ZHR is 4 times larger than those reported optically by Vida et al. (2024), assuming the same mass distribution function index. The difference in the peak time and the peak ZHR indicates that two different populations where observed by radar and video methods.

We have also presented a comparisons with GMN observations and dynamical models and in summary, the model presented by Egal et al. (2019) allows bringing particles of a few mm in size near the Earth during the maximum peak reported by GMN, and although older trails, carrying larger particles, may explain the peak observed by GMN, it indicates that SAAMER-OS' observations are better explained by a contribution from the 1974 trail, further showing that the radar and video peaks were produced by two distinct meteoroid populations.

Acknowledgements. Support for this work, as well as SAAMER-OS' operation, is provided by NASA's Planetary Science Division Research Program, through ISFM work package Exospheres, Ionospheres, Magnetospheres Modeling at Goddard Space Flight Center and NASA Engineering Safety Center (NESC) assessment TI-17-01204. G.S. is a member of the Oeschger Center for Climate Change Research (OCCR). D.V. was supported in part by NASA Cooperative Agreement 80NSSC21M0073 and by the Natural Sciences and Engineering Research Council of Canada.

References

Baggaley, W. J., Bennett, R. G. T., Steel, D. I., et al. 1994, QJRAS, 35, 293
Brown, P., Weryk, R. J., Wong, D. K., & Jones, J. 2008, Earth Moon Planets, 102, 209
Brown, P., Wong, D. K., Weryk, R. J., & Wiegert, P. 2010, Icarus, 207, 66
Bruzzone, J. S., Brown, P., Weryk, R. J., & Campbell-Brown, M. D. 2015, MNRAS, 446, 1625
Bruzzone, J. S., Janches, D., Jenniskens, P., Weryk, R., & Hormaechea, J. L. 2020, Planet. Space Sci., 188, 104936
Bruzzone, J. S., Weryk, R. J., Janches, D., et al. 2021, Planet. Sci. J., 2, 56
Crifo, J. F., & Rodionov, A. V. 1997, Icarus, 127, 319
Dawkins, E. C. M., Stober, G., Carrillo-Sánchez, J. D., et al. 2023, Planet. Space Sci., 238, 105796
Egal, A., Wiegert, P., Brown, P. G., et al. 2019, Icarus, 330, 123
Egal, A., Wiegert, P., Brown, P. G., Campbell-Brown, M., & Vida, D. 2020, A&A, 642, A120
Farnham, T. L., Kelley, M. S. P., Knight, M. M., & Feaga, L. M. 2019, ApJ, 886, L24
Fritts, D. C., Janches, D., Iimura, H., et al. 2010, J. Geophys. Res. (Atmos.), 115, 18112
Janches, D., Close, S., Hormaechea, J. L., et al. 2015, ApJ, 809, 36
Janches, D., Bruzzone, J. S., Weryk, R. J., et al. 2020, ApJ, 895, L25
Janches, D., Bruzzone, J. S., Weryk, R. J., Hormaechea, J. L., & Brunini, C. 2023, Planet. Sci. J., 4, 165
Jenniskens, P., Gural, P. S., Dynneson, L., et al. 2011, Icarus, 216, 40
Maslov, M. P., & Muzyko, E. I. 2017, Earth Moon Planets, 119, 85
Moulane, Y., Jehin, E., Manfroid, J., et al. 2023, A&A, 670, A159
Pokorný, P., Sarantos, M., & Janches, D. 2017, ApJ, 842, L17
Schult, C., Brown, P., Pokorný, P., Stober, G., & Chau, J. L. 2018, Icarus, 309, 177
Stober, G., Weryk, R., Janches, D., et al. 2023, Planet. Space Sci., 237, 105768
Vaubaillon, J., Egal, A., Desmars, J., & Baillie, K. 2020, WGN, J. Int. Meteor Organ., 48, 29
Vaubaillon, J., Ye, Q. Z., Egal, A., Sato, M., & Moser, D. E. 2023, A&A, 680, A10
Vida, D., Scott, J. M., Egal, A., et al. 2024, A&A, 682, A20
Vondrak, T., Plane, J. M. C., Broadley, S., & Janches, D. 2008, Atmos. Chem. Phys., 8, 7015
Weryk, R. J., & Brown, P. G. 2013, Planet. Space Sci., 81, 32
Ye, Q., & Jenniskens, P. 2022, arXiv e-prints, [arXiv:2209.10654]
Ye, Q.-Z., Hui, M.-T., Brown, P. G., et al. 2016, Icarus, 264, 48
Ye, Q., Vaubaillon, J., Sato, M., & Maslov, M. 2021, ATel, 14947